Biosensors and Bioelectronics 188 (2021) 113314

Contents lists available at ScienceDirect

Biosensors and Bioelectronics

journal homepage: www.elsevier.com/locate/bios

Streptavidin-functionalized terahertz metamaterials for attomolar exosomal microRNA assay in pancreatic cancer based on duplex-specific nuclease-triggered rolling circle amplification

Xinyu Zhan [a,1], Sha Yang [a,1], Guorong Huang [a], Lihua Yang [a], Yang Zhang [b], Huiyan Tian [a], Fengxin Xie [a], Marc Lamy de la Chapelle [c], Xiang Yang [a,**], Weiling Fu [a,*]

[a] Department of Laboratory Medicine, Southwest Hospital, Third Military Medical University (Army Medical University), Chongqing, 400038, China
[b] Department of Laboratory Medicine, Chongqing University Cancer Hospital, Chongqing, 40038, China
[c] Institut des Molécules et Matériaux Du Mans (IMMM-UMR CNRS 6283), Université Du Mans, Avenue Olivier Messiaen, 72085, Le Mans, France

ARTICLE INFO

Keywords:
Terahertz metamaterials
MicroRNA-21
Gold nanoparticles
Streptavidin

ABSTRACT

Exosomal microRNA (miRNA) is a promising non-invasive biomarker for liquid biopsies. Herein, we fabricated a terahertz (THz) metamaterial biosensor that comprises an array of gold (Au) discs surrounded by annular grooves for exosomal miRNA assays based on duplex-specific nuclease (DSN)-triggered rolling circle amplification (RCA). In this strategy, the target miRNA is captured by a probe P0 immobilized on magnetic beads (MBs); it then repeatedly releases a primer P1 under the action of DSN, which acts as a highly specific initiator of the subsequent RCA step utilizing biotin-dUTP. After target recycling and nucleic acid amplification, the biotinylated amplification products were captured by the streptavidin (SA)-functionalized THz metamaterials, and further conjugated to SA-modified AuNPs that permit formation of a trimeric complex of SA-biotinylated RCA products-AuNP. The complex population scales with the starting concentration of the target miR-21, resulting in a red shift of the resonance peak of the THz metamaterials. This biosensor can lead to highly specific and sensitive detection with one-base mismatch discrimination and a limit of detection (LOD) down to 84 aM. Significant distinctions are seen in the frequency shifts for exosomal miR-21 quantitation in clinical plasma samples between pancreatic cancer patients and healthy controls. The frequency shifts of the THz metamaterials are consistent versus the reverse transcription-polymerase chain reaction (RT-PCR) results, illustrating the applicability and accuracy of our assay in real clinical samples.

1. Introduction

MicroRNA (miRNA) is a promising non-invasive biomarker for cancer diagnosis due to its close interactions with parental tumor cells (Thind and Wilson, 2016). Particularly, exosomal miRNAs reflect specific physiological conditions and the functions of their parental cells via the endosomal origin. Their detection in body fluids could thus lead to reliable early-stage diagnosis and may serve as a novel biomarker for the early cancer diagnosis (Li et al., 2019). However, detecting specific miRNAs from total exosomal RNAs remains challenging due to their high sequence homology, small size, and low abundance. The reverse transcription-polymerase chain reaction (RT-PCR) can characterize miRNA expression down to the fM level, but it needs rigorous operating conditions and strict thermal cycles. Other biosensing methods have emerged, such as fluorescence (Wang et al., 2020), electrochemical biosensors (Cheng et al., 2020) and surface-enhanced Raman spectroscopy (SERS) (Pang et al., 2019), but some drawbacks such as poor stability and tedious experimental procedures still exist. Hence, a sensitive, reliable, and convenient strategy for exosomal miRNA detection is highly desirable.

Terahertz (THz) spectroscopy has been evaluated as a promising biosensing method due to its keen sensitivity to biomolecular interactions and the high signal-to-noise ratio (Yang et al., 2016). THz spectroscopy has good performance in cell and tissue profiles (Lee et al.,

* Corresponding author.
** Corresponding author.
E-mail addresses: yangxiang@tmmu.edu.cn (X. Yang), weiling_fu@126.com (W. Fu).
[1] XY.Z. and S. Y. contributed equally to this work.

https://doi.org/10.1016/j.bios.2021.113314
Received 9 April 2021; Accepted 4 May 2021
Available online 9 May 2021

2020); however, the size mismatch between biomolecules and THz waves (30–3000 μm) is a hurdle for effective biomolecular biosensing. To address this issue, THz metamaterials have been recently utilized for enhancing THz-biomolecule interactions to achieve higher sensitivities (Xu et al., 2017). These periodic artificial electromagnetic media composed of subwavelength microstructure arrays exhibit permittivity or refractive index changes caused by the deposition of extraneous substances, leading to resonance frequency shifts. Thus, THz metamaterials have been exploited for accurate detection of glucose (Roh et al., 2019), antibiotics (Xie et al., 2019), bacteria (Yoon et al., 2020), and viruses (Park et al., 2017).

THz metamaterials have also garnered considerable attention for nucleic acid detection due to the insufficient sensitivity of free-space THz detection (Xu et al., 2017). Specifically, large amounts of nucleic acids (micromolar level) are required for reliable signal response (Tang et al., 2015). To improve the detection sensitivity, our previous study used rolling circle amplification (RCA) to isothermally amplify bacterial DNA and achieve a limit of detection (LOD) of 60 pM (Yang et al., 2017). By comparison, coupling RCA with THz metamaterials realized a significantly improved LOD, reaching as low as 2.77 fM for bacterial DNA (Yang et al., 2020), showing another 10^4-fold improvement. The improved sensitivity has been demonstrated using this methodology, but the interference of complex matrices in the clinical samples remains an obstacle before applying THz metamaterials in applications.

To guarantee trace exosomal miRNA detection with a high level of sequence homology, Kim and colleagues recently reported a duplex-specific nuclease (DSN)-triggered signal amplification strategy in biosensing (Kim et al., 2017). Here, the DSN can accurately distinguish and specifically degrade DNA (up to one mismatch) in a DNA-RNA duplex while keeping the RNA intact to realize circulation. The DSN-triggered cascade can achieve fairly low LOD via target recycling and RCA signal amplification. Thus, this strategy enables trace exosomal miRNA capture and amplification with high specificity and sensitivity simultaneously (Kim et al., 2017).

However, crystalline salts introduced via the nucleic acid amplification buffer will introduce unwanted scattering of the THz waves on the surface of THz metamaterials (Berrier et al., 2012). Magnetic beads (MBs) were used to purify the amplification products via magnetic separation in the previous study (Yang et al., 2020). Nevertheless, this strategy inevitably resulted in high coverage signal of the control sample (without amplification) due to the high refractive index of MBs. Furthermore, amplification products after magnetic separation are unequally distributed on the surface of the THz metamaterials during the sample process. In other words, the capillary flow out from the center of the liquid drop brings suspended biomaterials to the edge as evaporation proceeds; this is the so-called “coffee ring index” (Deegan et al., 1997). To address these issues, streptavidin (SA) can be selected as a receptor to capture amplification products, taking advantage of its non-covalent binding ability with biotin and its low refractive index. This approach can also ingeniously ensure uniform liquid drop distribution on the THz metamaterial surface through SA functionalization and sample incubation.

Herein, we established a THz metamaterial biosensor for sensitive and specific exosomal miRNA assay in the plasma of pancreatic cancer patients based on DSN-triggered RCA using miRNA-21 (miR-21) as the target. After target recycling and isothermal amplification, the liquid phase amplification products were incubated for SA-biotin binding to ensure uniform sample distribution and thoroughly washed to remove the salt ions from the amplification system. A frequency shift in the resonance peak of the THz metamaterials could be observed due to coverage of the RCA products, which can be further boosted by the conjugated Au nanoparticles with high refractive index. Its practical value was validated for detecting clinical plasma samples from pancreatic cancer patients. These shifts are consistent with the gold standard method RT-PCR, illustrating the accuracy of proposed biosensor for exosomal miRNA assays in real biological samples, which may serve as a general methodology for nuclear acid biosensing.

2. Experimental section

2.1. Chemicals and reagents

All custom-prepared, HPLC-purified oligonucleotides are shown in Table S1. Information regarding reagents are described in the Supporting Information (SI).

2.2. DSN-triggered RCA

The functionalized MBs (preparation procedures are described in the SI) were added to 10 μL DSN reaction system containing 0.1 μL DSN (0.5 U/μL), 1 μL target miR-21 (10 μM), 1 μL master buffer (500 mM Tris-HCl, pH 8.0; 50 mM $MgCl_2$; 10 mM DTT), and 7.9 μL H_2O. These mixtures were incubated at 55 °C for 2 h using a thermomixer. After magnetic separation, the residual solution was inactivated at 100 °C for 20 min to obtain the RCA primer P1. Next, the RCA reaction was performed at 65 °C for 2 h in a 50 μL solution containing 10 μL P1; 1 μL Bst 3.0 DNA polymerase; 1 μL RCA template (10 μM); 2 μL each of dATP, dGTP, dCTP, and biotin-11-dUTP; 5 μL isothermal amplification buffer; 1 μL $MgSO_4$; and 24 μL H_2O. Heat inactivation of RCA was performed at 80 °C for 5 min.

Next, 25 μL of RCA products was cultured with 10 μL KCl (500 mM) and 15 μL TE at 37 °C for 30 min and then added to 2 μL hemin (2 μM, dissolved in DMSO) at 37 °C for 30 min. Colorimetric reactions were performed at 37 °C for 30 min upon addition of 50 μL TMB.

2.3. Fabrication and functionalization of THz metamaterials

The fabrication steps of the THz metamaterials comprise an array of Au discs surrounded by annular grooves are as follows: 1) a dielectric layer of silicon dioxide with a thickness of 2 μm was processed on the surface of the high-resistivity silicon wafer substrate using magnetron sputtering; 2) a part of the silicon dioxide layer was then removed by ion beam etching to form annular grooves around the discs; 3) a 200 nm-thick Au/Cr layer was deposited and fabricated on the annular grooves and the discs using a standard photolithography technique in which Cr functioned as an adhesion layer. The arrays of Au discs are designed to be polarization independent to assure detection stability and reproducibility. Detail procedures of preparing SA-functionalized THz metamaterials are described in the SI.

2.4. Terahertz measurements of rolling circle amplification (RCA) products

Twenty-five microliters of RCA products were dropped on the metamaterial and incubated for 10 min. After rinsing with deionized water three times to remove impurities like salt ions and proteins, 5 μL of SA-modified gold nanoparticles (AuNPs) (50 μg/mL) were incubated for 10 min to form the trimeric complex of SA-biotinylated RCA products-AuNP (Fig. S1). The biosensor was then rinsed with deionized water three times and dried with nitrogen (dried at 50 °C for 10 min) for THz measurement. All THz measurements were performed at three different times in reflection mode.

A frequency shift was calculated by $\Delta f = f_{\text{miR-21}} - f_{\text{SA-functionalized MM}}$ of which $f_{\text{miR-21}}$ represents the resonance peak frequency of the sample, and $f_{\text{SA- functionalized MM}}$ symbolizes the resonance peak frequency of the SA-functionalized metamaterial biosensor without a target.

2.5. Extraction and characterization of exosomes

The plasma specimens of 20 pancreatic cancer patients and 20 healthy controls were collected from the Southwest Hospital of Army Medical University (Chongqing, China). The study was approved by the

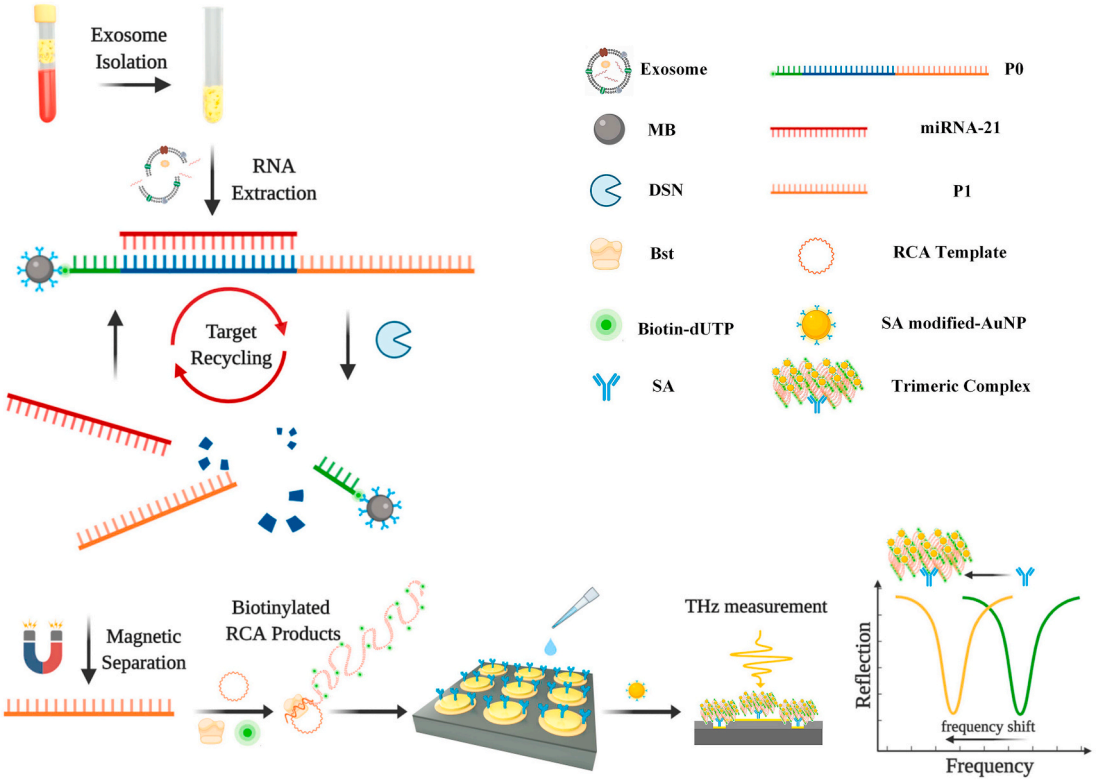

Fig. 1. Schematic diagram of streptavidin-functionalized THz metamaterials for exosomal miRNA-21 assay based on DSN-triggered RCA.

ethics committee of the hospital. Exosomes and exosomal microRNAs were extracted from 1 mL blood sample according to protocols of the exoEasy Maxi Kit and exoRNeasy Midi/Maxi Kit. As shown in Table S2, there was no significant difference in gender and age between pancreatic cancer patients and healthy controls. The isolated exosomes were observed using TEM and were analyzed by NTA. Surface proteins from exosomes and PANC-1 cells were analyzed by western blot.

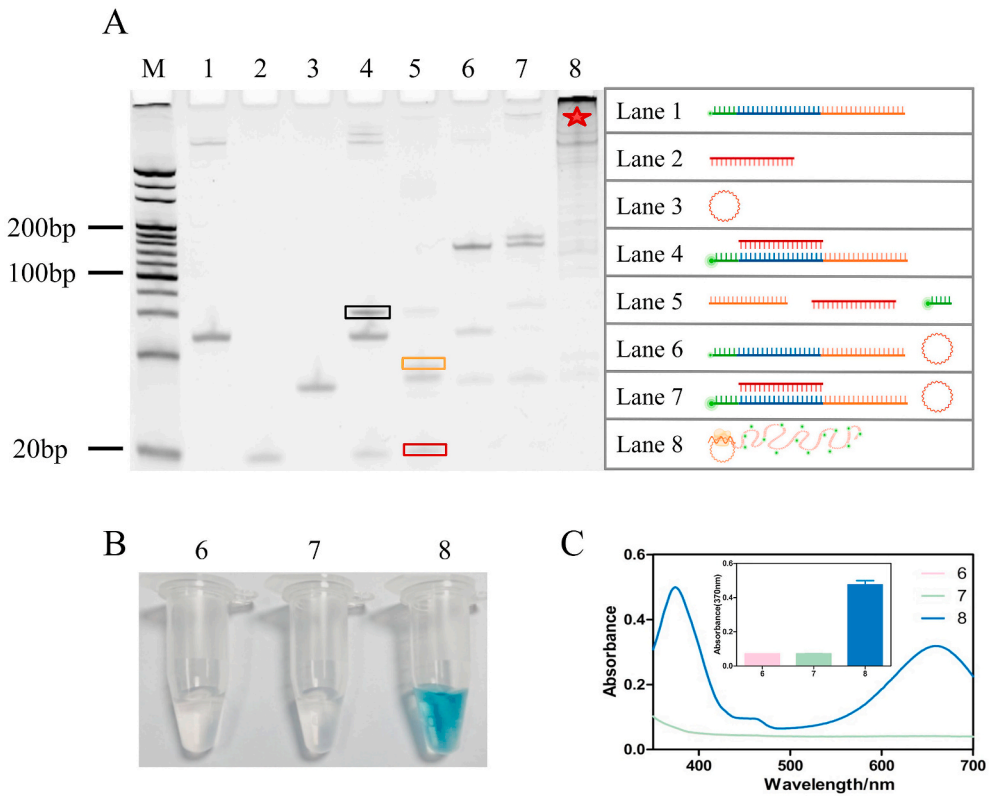

Fig. 2. The DSN-triggered RCA strategy. A) PAGE analysis. Lane M: 20 bp DNA ladder, lane 1: P0, lane 2: miR-21, lane 3: RCA template, lane 4: P0 bound with miR-21, lane 5: P0 bound with miR-21 and treated with DSN, lane 6: RCA employing lane 1 as the primer, lane 7: RCA employing lane 4 as the primer, lane 8: RCA employing lane 5 as the primer. B) Colorimetric assay of G-quadruplex DNase catalysis. C) Absorption spectra of colorimetric assay from 350 to 700 nm. The inset is the image of the corresponding histogram with an error bar at an absorbance of 370 nm.

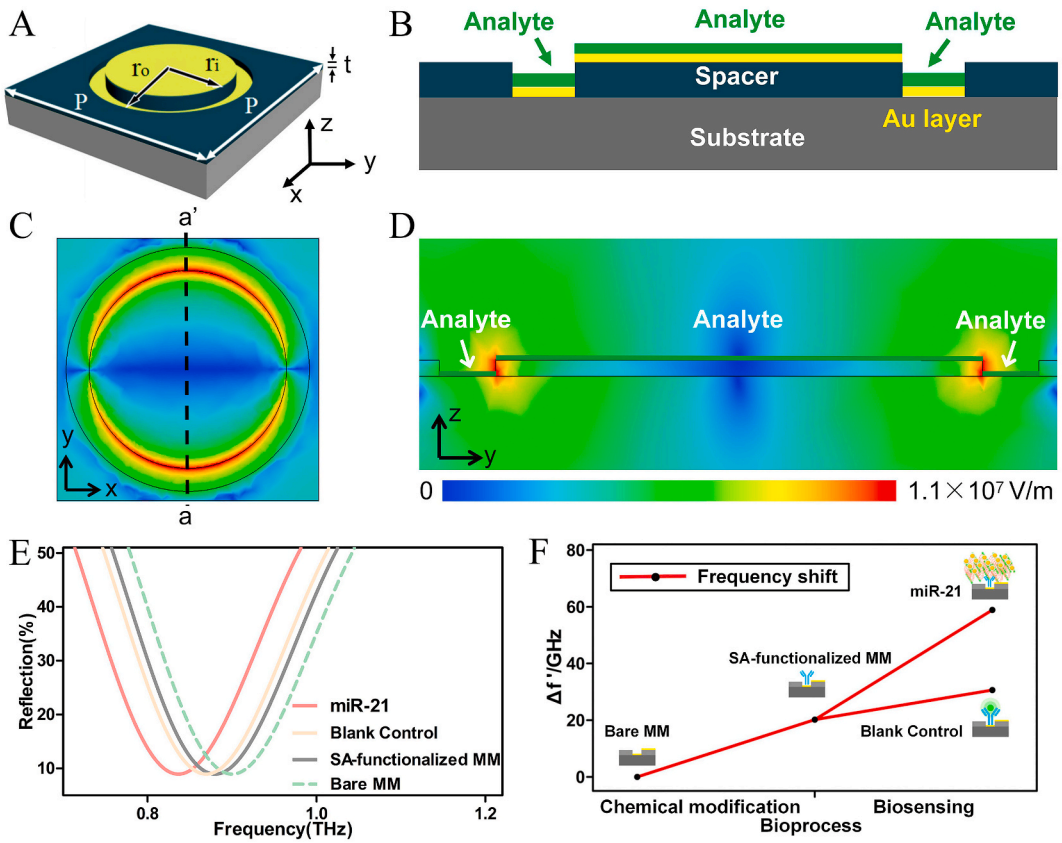

Fig. 3. Establishment of the THz metamaterial biosensor. A) A schematic diagram a structure unit of the THz metamaterials. Dimensions: P = 114 μm, r_o = 53 μm, r_i = 43 μm, t = 2 μm. B) The cross-sectional view of the THz metamaterials showing the analyte distribution. C) The top view of the electric field distribution. D) The cross-sectional view of electric field distribution (as indicated by the dotted line in the Fig. 3C). E) THz measurements of different samples. Bare MM: bare metamaterials; SA-functionalized MM: SA-functionalized metamaterials. Blank Control: buffer without miR-21. F) The corresponding THz frequency shifts (Δf') of Fig. 3E. $\Delta f' = f - f_{\text{Bare MM}}$ of which f represents the resonance peak frequency of SA-functionalized MM, blank control, or miR-21, and $f_{\text{Bare MM}}$ symbolizes the resonance peak frequency of the bare metamaterials.

2.6. RT-PCR analysis

The whole miRNAs were reverse-transcribed to complementary DNA (cDNA) using the miScript II RT Kit. After adding the template miRNAs, the reaction solution was incubated at 37 °C for 60 min, and the reverse transcriptase was inactivated at 95 °C for 5 min. Subsequently, the thermal cycling states of RT-PCR were proceeded with the mix via miScript SYBR Green PCR Kit as follows: 95 °C for 15 min followed by 40 cycles at 94 °C for 15 s, 55 °C for 30 s, and 70 °C for 30 s.

3. Results and discussion

3.1. Design of a THz metamaterial biosensor based on DSN-triggered RCA

As shown in Fig. 1, the proposed THz metamaterial biosensor consists of target recycling via DSN, isothermal amplification by RCA, and a product assay by SA-functionalized THz metamaterials. The biotinylated probe P0 comprises a coupling part (green part), recognition part (blue part), and primer part (orange part, P1) at different segments (Fig. S2). The 5′ end of P0 is the coupling part and was modified with MBs via the SA-biotin system. The recognition part is complementary to the target for DSN-specific recognition and degradation. In the presence of target exosomal miR-21, the recognition part of the functionalized MBs can hybridize with the target to form DNA/RNA duplexes, which can then be specifically recognized by DSN. The subsequent recognition part can then be degraded, whereas the target miR-21 remains intact to continue the next cycle. After DSN occurs, the 3' end of P0 can turn into P1 triggering RCA as the primer, upon addition of the RCA template, the Bst DNA polymerase and dNTPs containing biotin-dUTP. Finally, the THz metamaterials functionalized with SA could easily recognize and capture biotinylated RCA products to cause a frequency shift. The localized electric field in the gaps of the THz metamaterials enhanced the interaction between the amplification products and the incident THz wave, which was further boosted by AuNPs via the large swings in the refractive index.

3.2. Feasibility of DSN-triggered RCA strategy

The feasibility of the DSN-triggered RCA strategy can be portrayed in 12% native polyacrylamide gel electrophoresis (PAGE) at 120 V for 45 min. As shown in Fig. 2A, the P0 (lane 1) bound with miR-21 (lane 2) to generate larger DNA/RNA duplexes (black frame, lane 4). After DSN-specific recognition and degradation, P1 (orange frame, lane 5) can be released, and miR-21 (red frame, lane 5) can be recycled. The RCA process could not be initiated with only adding P0 (lane 6). Without the DSN effect, RCA still did not occur (lane 7). Only in the presence of DSN, RCA was triggered as expected to generate the RCA products on the top of lane 8; the distinct band (red star) has much lower mobility.

To further validate the presence of RCA products, the C-rich RCA template was designed in advance and can produce massive G-rich oligonucleotide sequences. In the presence of K^+, G-rich oligonucleotides can fold into G-quadruplex units and capture hemin to form a DNase with horseradish peroxidase activity to further catalyze colorless tetramethyl benzidine (TMB) into a visible-blue product (oxTMB), as shown in Fig. 2B and C. The solutions of lanes 6–8 in Fig. 2A proceeded through this colorimetric assay and the optical densities were recorded

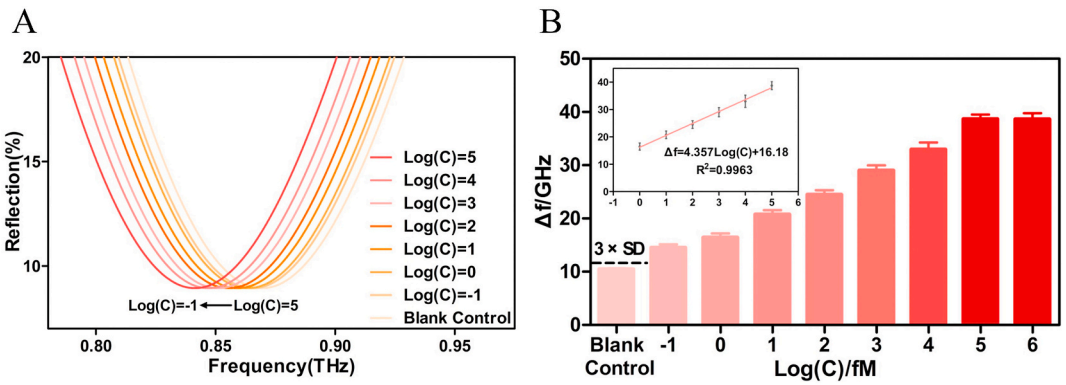

Fig. 4. Sensitivity of the THz metamaterial biosensor. A) THz reflections for miR-21 detection of different concentrations. B) The histogram of the THz frequency shifts (Δf). The insert is the corresponding calibration plot for the THz frequency shifts (Δf) vs Log(C)/fM. Each point represents the average value of three independent assays with error bars indicated.

at 350 nm–700 nm. The results show that only lane 8 became blue with a maximum absorbance much higher than those of lane 6 and lane 7, thus verifying the successful accomplishment of the RCA process.

3.3. Detection of miR-21 by the THz metamaterial biosensor

Fig. 3A shows a cell of the fabricated THz metamaterials containing an Au disc surrounded by an annular groove. The analyte of the trimeric complex of SA-biotinylated RCA products-AuNP can be captured on the surface of the Au disc but also to the Au layer inside the groove via SA–biotin linkage (Fig. 3B). At the resonance, the incident THz electrical field induces a large accumulation of the surface charges between the two metal layers causing an extremely strong electrical field on the side wall of the center cylinder in the annular grooves. Following the dipole resonant mode, the maximum value of the electrical field distribution appears at both ends of the center cylinder along the y axis (Fig. 3C) as well as on the side wall of the cylinder and the neighboring area in the annular groove in the z-direction (Fig. 3D). The excited hot-spots spatially overlapped with the analyte, which greatly enhanced the interactions between THz waves and the analyte (Zhou et al., 2019).

As shown in Fig. 3E and F, the bare THz metamaterials produced a resonance peak near 0.9 THz, and SA was then chemically grafted on the Au film of the THz metamaterial surface, which exhibited a frequency shift confirming successful functionalization. Next, 800 nM of SA was used to saturate the surface of the THz metamaterials (Fig. S3), and eliminate non-specific interactions between the analyte and THz metamaterial surface. We measured the biotinylated RCA products on the bare THz metamaterial chip (without streptavidin) and the SA-coated THz metamaterial chip. The results demonstrated that streptavidin can not only guarantee the uniform sample distribution but also specifically capture the biotinylated RCA products on the chip surface for biosensing (see details in SI). In the presence of target miR-21, the biotinylated RCA products conjugated with AuNPs were captured by the SA-functionalized THz metamaterials giving rise to a further response of 38.7 ± 1.4 GHz. In contrast, a slight frequency shift of the blank control (10.4 ± 0.3 GHz) occurred due to the combination of biotin-dUTP with SA. This phenomenon may be attributable to the high refractive index of nanomaterials and the fact that RCA products consist of a large number of THz-sensitive intermolecular interactions (hydrogen bonds and van der Waals), biomolecular vibrations, and rotations. In contrast, the hybridized biotin-dUTPs without AuNPs in the blank control result in only a relatively small frequency shift.

3.4. Optimization of experimental conditions

We next optimized the performance of the biosensor. As illustrated in Fig. S4A, the frequency shift reached an equilibration state at 15 μM P0. Hence, 15 μM was chosen as the optimum concentration of P0 in the DSN step. Likewise, 2 h of DSN reaction time and 2 h of RCA reaction time were selected for the optimum conditions where frequency shifts plateaued (Fig. S4B and Fig. S4C). The whole process takes about 4.5 h, which is comparable with other biosensors using dual-amplification methods (Table S3). Of the 1.4 nm, 10 nm, and 20 nm AuNPs, the 1.4 nm AuNPs exhibited more frequency shifts, as shown in Fig. S4D, possibly due to their more suitable size to be conjugated with RCA products. In addition, 50 μg/mL was chosen as the optimum concentration of AuNPs because redundant AuNPs inhibited the hybridization as a result of the accretion of steric hindrance in the three-dimensional space (Fig. S4E).

3.5. Sensitivity of the THz metamaterial biosensor

As the concentration of miR-21 increased, the THz metamaterial biosensor produced a gradual frequency shift towards the left in response under the optimum conditions (Fig. 4A). A favorable linear relationship was discovered between THz frequency shift (Δf) and the logarithmic value of the target concentration (Log(C)), ranging from 1 fM to 100 pM (Fig. 4B). The linear fitting equation was $\Delta f = 4.375$ Log (C)+16.18, with a correlation coefficient (R^2) of 0.9963. The LOD was 84 aM as calculated by 3-fold standard deviation (SD) more than the blank control. This was comparable equal to or better than the LODs of the other methods reported such as SERS, fluorescence, or electrochemical biosensors (Table S4). The tunable detection range and satisfactory sensitivity indicated a favorable synergy between the DSN-triggered RCA strategy and the annular grooves of the THz metamaterials, which are endowed with strong localized electric fields. The biotinylated amplification products conjugated to AuNPs and led to nanoparticle-DNA complexes with high refractive index. Coverage of the trimeric complex (SA-biotinylated RCA products-AuNP) on the THz metamaterials led to an obvious THz response as a function of the target concentration. Moreover, the relative standard deviation (RSD) of the target miR-21 detection ranged from 3.73% to 7.88% (from 100 aM to 1 nM; Table S5), thus indicating good repeatability of the proposed THz metamaterial biosensor; this may be attributable to the uniform sample distribution on the surface and the low background interference from sample matrix.

3.6. Specificity of the THz metamaterial biosensor

The specificity of this proposed biosensor was evaluated before practical applications. Several miRNAs of 10 pM containing single, double and triple-base mismatched targets (SMT, DMT and TMT, respectively), other types of miRNAs (miR-25, miR-107, miR-145) (Table S1), and the mixture including miR-25, miR-107, miR-145, and

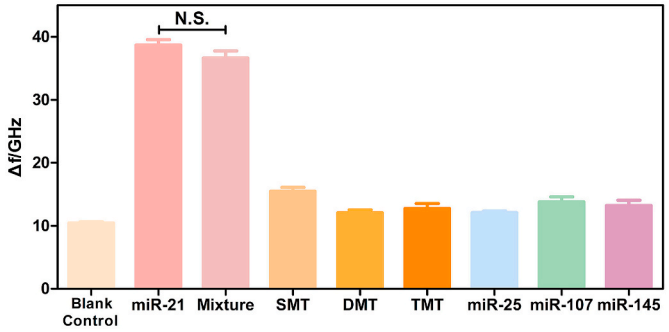

Fig. 5. Specificity verification of the THz metamaterial biosensor. Blank Control: buffer without mi21; SMT: single-base mismatched target; DMT: double-base mismatched target; TMT: triple-base mismatched target; Mixture: miR-25, miR-107, miR-145, and miR-21 at 1:1:1:1. N.S., not significant ($P > 0.05$). The error bars represent the standard deviations of three independent experiments.

miR-21 with the proportion of 1:1:1:1 were added and detected by this biosensor. Fig. 5 shows the THz frequency shifts induced by non-complementary targets like miR-25, miR-107, miR-145 are not prominent. The blank control has a frequency shift around 10 GHz due to the limited combination of biotin-dUTP with surface-coated SA during THz measurements. The mixture of miRNAs and miR-21 induced a much higher frequency shift than other individual miRNAs; however, this is not significantly different from the one measured for the target miR-21 alone ($P > 0.05$), suggesting that the presence of other miRNAs in the sample did not disturb the detection of miR-21. Moreover, frequency shifts of SMT, DMT, and TMT remained significantly lower than the frequency shift of miR-21 due to the specific target binding. Theoretically, the mismatch sequences cannot trigger DSN and form the trimeric complex of SA-biotinylated RCA products-AuNP. But the DSN has a small degradation effect on the DNA part of the DNA-RNA complex even if it is not perfectly paired. Nevertheless, the target miR-21 could still be accurately recognized to coexist with similar miRNAs, possibly due to the accurate identification capacity of DSN.

3.7. Clinical application of the THz metamaterial biosensor

The proposed biosensor was next verified for clinical practicability by detecting exosomal miR-21 from the plasma of pancreatic cancer patients. The extracted exosomes had a typical cup or saucer-like vesicle structure with an approximate diameter of 100 nm, as observed by transmission electron microscopy (TEM; Fig. 6A). Besides, nanoparticle tracking analysis (NTA) in Fig. 6B showed that median size of the obtained exosomes was about 109 nm. The western blot in Fig. 6C shows apparent bands of surface proteins CD9 and CD63 but there is no calnexin band, which confirmed the existence of exosomes versus the corresponding results of PANC-1 cells. The above characterizations for the morphology, size and proteins of exosomes are consistent with previous reports (Miao and Tang, 2020), indicating successfully extraction of exosomes with highly purity. As shown in Table S2, the Δf measurement of pancreatic patients (n = 20) was about 27.8 ± 6.5 GHz compared to 21.8 ± 4.2 GHz for healthy controls (n = 20). Statistical analysis showed significantly higher THz frequency shifts for miR-21 ($P < 0.01$ = in pancreatic cancer samples versus healthy controls (Fig. 6D)), thus illustrating the potential value of the proposed biosensor to detect pancreatic cancer. Some pancreatic cancer patients may have similar miR-21 expression levels as healthy controls due to their different stages, pathological types, and individual differences (Lai et al., 2017). The feasibility of our biosensor to statistically distinguish the two groups could be demonstrated using miR-21 as the target. For further

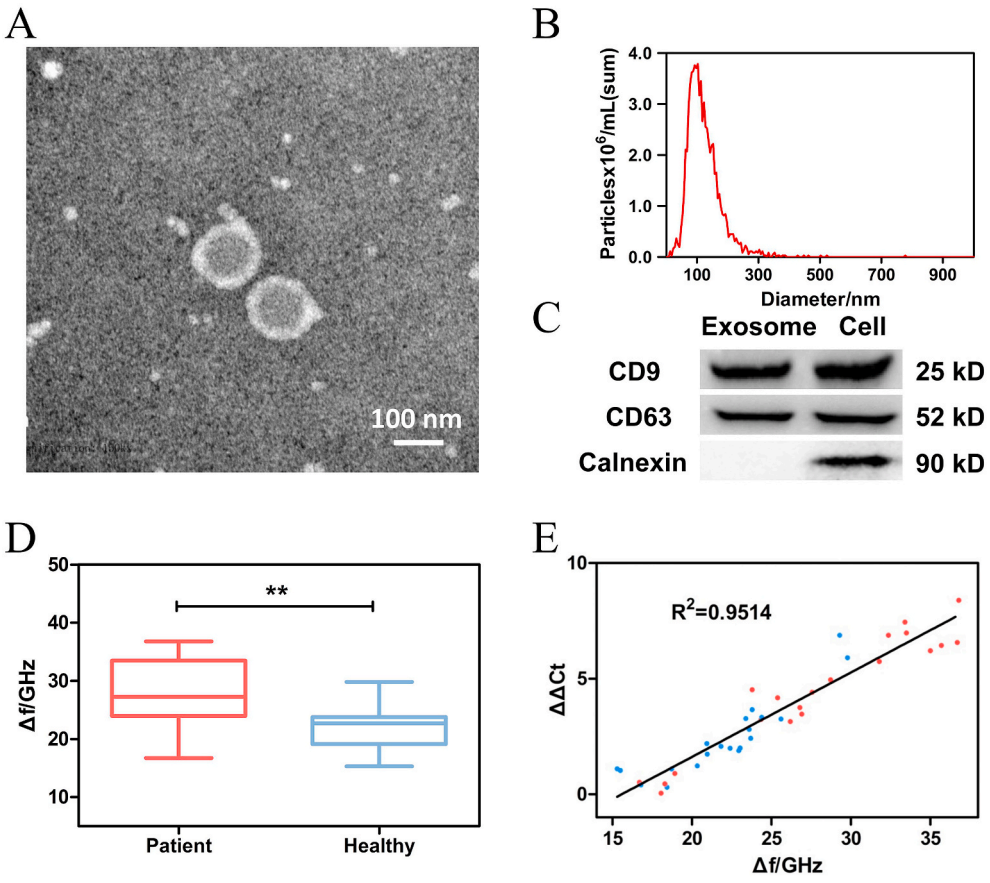

Fig. 6. Clinical application of the THz metamaterial biosensor. A) TEM image and B) nanoparticle tracking analysis (NTA) of the obtained exosomes. C) Western blot bands of CD9, CD63 and Calnexin in PANC1 cells and obtained exosomes. D) Detection efficiency of the THz metamaterial biosensor on clinical samples of pancreatic cancer patients and healthy controls. $^{**}P < 0.01$. E) Consistency between RT-PCR and the THz metamaterial biosensor for the detection of exosomal miR-21. The red dots represent the cancer patients and the blue dots represent the healthy controls. (For interpretation of the references to color in this figure legend, the reader is referred to the Web version of this article.)

diagnosis of pancreatic cancer patients located in the overlaps between the two groups (e.g., $\Delta f = 22$ GHz), multiple targets detection via probe design are envisioned to improve its diagnostic efficiency.

To verify the accuracy of the proposed biosensor, the frequency shifts of clinical samples were compared with the RT-PCR gold standard method using miR-39 as an external control. After the reaction, the ΔΔ threshold cycle (ΔΔ Ct) value of different concentrations of miR-21 in RT-PCR analysis was calculated via the Δ threshold cycle (Δ Ct) of the patient group minus the Δ Ct of the healthy group. The template exosomal miR-21 was also qualified via the biosensor, and the consistency of these methods was evaluated by comparing the relative expression quantity (ΔΔ Ct) and THz frequency shift of exosome-derived miR-21 (Fig. 6E). The two methods agree well with an R^2 value of 0.9514, thus illustrating the reliability and practicability of our assay in clinical samples. Compared to the recently reported biosensors for exosomal miRNAs detection applied to clinical samples (Table S6), the proposed THz metamaterial biosensor has good sensitivity and selectivity, while maintaining well repeatability (Table S7). In this work, the THz metamaterial biosensor with good performance is simple and reliable, which enhances its potential for clinical applications.

4. Conclusion

In summary, we developed a novel THz metamaterial biosensor for exosomal miR-21 assay using a dual signal amplification strategy by coupling DSN-triggered RCA with AuNP-enhanced THz metamaterials. Under the optimum conditions, this biosensor offers a highly sensitive LOD of 84 aM with a linear detection range from 1 fM to 100 pM. For specificity, even a single-base mismatch and target miR-21 interfering miRNA-mixture can be recognized. To the best of our knowledge, this is the first use of THz metamaterials for cancer diagnosis of clinical samples. An unambiguous difference in frequency shifts can be found between pancreatic cancer patients versus healthy controls. The results were consistent with the current gold standard method RT-PCR, illustrating the robustness of THz metamaterials for absolute quantification of mature specific miRNA in real biological samples. The proposed THz metamaterial biosensor has good intrinsic benefits: it is label-free, simple to process, and features easy procedures. We now separated DSN-triggered RCA and THz assays to improve the amplification efficiency whereas increased the complexity; in future work, an integrated assay platform should be required for practical applications whereby *in situ* nucleic acid amplification, conjugation of nanoparticles, and THz measurement can be successively conducted. In this direction, the proposed method can be eventually used for early diagnosis and therapeutic monitoring of various cancers.

Declaration of competing interest

The authors declare that they have no known competing financial interests or personal relationships that could have appeared to influence the work reported in this paper.

Acknowledgments

This work was supported by National Natural Science Foundation of China (81802118) and the Military logistics scientific research project (AWS17J010).

Appendix A. Supplementary data

Supplementary data to this article can be found online at https://doi.org/10.1016/j.bios.2021.113314.

References

Berrier, A., Schaafsma, M.C., Nonglaton, G., Bergquist, J., Rivas, J.G., 2012. Selective detection of bacterial layers with terahertz plasmonic antennas. Biomed. Opt Express 3 (11), 2937–2949.
Cheng, W., Ma, J., Cao, P., Zhang, Y., Xu, C., Yi, Y., Li, J., 2020. Enzyme-free electrochemical biosensor based on double signal amplification strategy for the ultra-sensitive detection of exosomal microRNAs in biological samples. Talanta 219, 121242.
Deegan, R.D., Bakajin, O., Dupont, T.F., Huber, G., Witten, T.A., 1997. Capillary flow as the cause of ring stains from dried liquid drops. Nature 389 (6653), 827–829.
Kim, E., Howes, P.D., Crowder, S.W., Stevens, M.M., 2017. Multi-amplified sensing of MicroRNA by a small DNA fragment-driven enzymatic cascade reaction. ACS Sens. 2 (1), 111–118.
Lai, X., Wang, M., McElyea, S.D., Sherman, S., House, M., Korc, M., 2017. A microRNA signature in circulating exosomes is superior to exosomal glypican-1 levels for diagnosing pancreatic cancer. Canc. Lett. 393, 86–93.
Lee, S.H., Shin, S., Roh, Y., Oh, S.J., Lee, S.H., Song, H.S., Ryu, Y.S., Kim, Y.K., Seo, M., 2020. Label-free brain tissue imaging using large-area terahertz metamaterials. Biosens. Bioelectron. 170, 112663.
Li, K., Chen, Y., Li, A., Tan, C., Liu, X., 2019. Exosomes play roles in sequential processes of tumor metastasis. Int. J. Canc. 144 (7), 1486–1495.
Miao, P., Tang, Y., 2020. Dumbbell hybridization chain reaction based electrochemical biosensor for ultrasensitive detection of exosomal miRNA. Anal. Chem. 92 (17), 12026–12032.
Pang, Y., Wang, C., Lu, L., Wang, C., Sun, Z., Xiao, R., 2019. Dual-SERS biosensor for one-step detection of microRNAs in exosome and residual plasma of blood samples for diagnosing pancreatic cancer. Biosens. Bioelectron. 130, 204–213.
Park, S.J., Cha, S.H., Shin, G.A., Ahn, Y.H., 2017. Sensing viruses using terahertz nano-gap metamaterials. Biomed. Opt Express 8 (8), 3551–3558.
Roh, Y., Lee, S.H., Kang, B., Wu, J.W., Ju, B.K., Seo, M., 2019. Terahertz optical characteristics of two types of metamaterials for molecule sensing. Opt Express 27 (13), 19042–19049.
Tang, M., Huang, Q., Wei, D., Zhao, G., Chang, T., Kou, K., Wang, M., Du, C., Fu, W.L., Cui, H.L., 2015. Terahertz spectroscopy of oligonucleotides in aqueous solutions. J. Biomed. Opt. 20 (9), 95009.
Thind, A., Wilson, C., 2016. Exosomal miRNAs as cancer biomarkers and therapeutic targets. J. Extracell. Vesicles 5, 31292.
Wang, R., Zhao, X., Chen, X., Qiu, X., Qing, G., Zhang, H., Zhang, L., Hu, X., He, Z., Zhong, D., Wang, Y., Luo, Y., 2020. Rolling circular amplification (RCA)-Assisted CRISPR/Cas9 cleavage (RACE) for highly specific detection of multiple extracellular vesicle MicroRNAs. Anal. Chem. 92 (2), 2176–2185.
Xie, L., Wang, C., Chen, M., Jin, B.B., Zhou, R., Huang, Y., Hameed, S., Ying, Y., 2019. Temperature-dependent terahertz vibrational spectra of tetracycline and its degradation products. Spectrochim. Acta Mol. Biomol. Spectrosc. 222, 117179.
Xu, W., Xie, L., Ying, Y., 2017. Mechanisms and applications of terahertz metamaterial sensing: a review. Nanoscale 9 (37), 13864–13878.
Yang, K., Yu, W., Huang, G., Zhou, J., Yang, X., Fu, W., 2020. Highly sensitive detection of Staphylococcus aureus by a THz metamaterial biosensor based on gold nanoparticles and rolling circle amplification. RSC Adv. 10 (45), 26824–26833.
Yang, X., Yang, K., Zhao, X., Lin, Z., Liu, Z., Luo, S., Zhang, Y., Wang, Y., Fu, W., 2017. Terahertz spectroscopy for the isothermal detection of bacterial DNA by magnetic bead-based rolling circle amplification. Analyst 142 (24), 4661–4669.
Yang, X., Zhao, X., Yang, K., Liu, Y., Liu, Y., Fu, W., Luo, Y., 2016. Biomedical applications of terahertz spectroscopy and imaging. Trends Biotechnol. 34 (10), 810–824.
Yoon, S.A., Cha, S.H., Jun, S.W., Park, S.J., Park, J.Y., Lee, S., Kim, H.S., Ahn, Y.H., 2020. Identifying different types of microorganisms with terahertz spectroscopy. Biomed. Opt Express 11 (1), 406–416.
Zhou, H., Yang, C., Hu, D., Li, D., Hui, X., Zhang, F., Chen, M., Mu, X., 2019. Terahertz biosensing based on bi-layer metamaterial absorbers toward ultra-high sensitivity and simple fabrication. Appl. Phys. Lett. 115 (14), 143507.